

**ENCLOSURE 2
ATTACHMENT 5**

SHINE MEDICAL TECHNOLOGIES, INC.

**SHINE MEDICAL TECHNOLOGIES, INC. APPLICATION FOR CONSTRUCTION PERMIT
RESPONSE TO REQUEST FOR ADDITIONAL INFORMATION**

ANL/CSE-14/11

**SHINE TARGET-SOLUTION CHEMISTRY: THERMODYNAMIC MODELING
OF SPECIATION, PRECIPITATE FORMATION, AND THE
CHEMICAL EFFECTS OF STAINLESS STEEL CORROSION**

CONTENTS

1	SCOPE.....	1
2	SUMMARY.....	2
3	METHODS	3
	3.1 Building the Thermodynamic Database.....	3
	3.2 Example of Saturation Index Calculation.....	5
	3.3 Speciation/Saturation State of Irradiated SHINE Solution.....	6
4	DISCUSSION.....	7
	4.1 Speciation and Saturation Calculations at Room Temperature	7
	4.2 Speciation and Saturation Calculations of Temperature Effect.....	7
	4.3 Reduction/Oxidation Relationships between Key Species	17
	4.4 Chemical Effects of Steel Corrosion.....	21
5	CONCLUSIONS AND RECOMMENDATIONS	26
6	REFERENCES	27

FIGURES

1	Concentrations of Key Elements in the Target Solution over a Four-Cycle Run.....	9
2	Variation of Saturation Indices with pH for the Target Solution Composition Shown in Table 1	12
3	Variation of Aqueous Speciation with pH for the Target Solution Composition Shown in Table 1	13
4	Saturation Index and Selected Speciation of Target Solution over a Range of Steady-State Concentrations of Dissolved Hydrogen Peroxide	14
5	Selected Examples of How Saturation Indices and Key Species Change over the Temperature Range 25°C to 100°C.....	15
6	Additional Examples of How Saturation Indices and Key Species Change over the Temperature Range 25°C to 100°C.....	16

FIGURES (Cont.)

7	First Example of Redox Relationships between Selected Species from Table 2	18
8	Second Example of Redox Relationships between Selected Species from Table 2	19
9	Third Example of Redox Relationships between Selected Species from Table 2	20
10	Examples of Measured Steel Corrosion rates for 304, 316, 347 Stainless Steels in Uranyl Sulfate, Copper Sulfate, and Ferrous Sulfate Solutions at Different Temperatures.....	23
11	Amount of Steel Corroded per Time Given Relevant Ranges of the Corrosion Rate and Corroding Surface Area per Solution Volume	23
12	Equilibrium Model Results for the Dissolution of 316 Stainless Steel in the SHINE Solution	24
13	Equilibrium Model Results for the Dissolution of 316 Stainless Steel in the SHINE Solution	25

TABLES

1	Input Solution Composition for Speciation Modeling.....	8
2	Speciation and Saturation State of Solution Composition Shown in Table 1	10
3	Nominal Composition of Stainless Steels Used in Modeling.....	22

SHINE TARGET-SOLUTION CHEMISTRY: THERMODYNAMIC MODELING OF SPECIATION, PRECIPITATE FORMATION, AND THE CHEMICAL EFFECTS OF STAINLESS STEEL CORROSION

1 SCOPE

The potential for precipitate formation in the SHINE target solution was a concern expressed by the Nuclear Regulatory Commission (NRC). Precipitates can form from several sources:

- Uranium-peroxide precipitation is being suppressed by the addition of 1-10 ppm FeSO_4 to the target solution; this technique is being verified by micro-SHINE experiments. Uranyl sulfate is extremely soluble.
- Precipitation of sulfate salts as fission and corrosion products build up in solution. Corrosion products will arise from corrosion of both Zircaloy-IV (the target-solution tank) and Type 316 stainless steel (lines, storage tanks, and equipment).

This study on the precipitate-formation concern is proceeding in two steps. In the first step, chemical modeling of the target solution is performed by using available computer codes to calculate saturation indexes for potential precipitating phases available in a thermodynamic data base. The second step, to be described in a separate report, is measurement of solubilities of components that the modeling suggests could precipitate in the SHINE target solution.

2 SUMMARY

The following results are from modeling the chemistry of the target solution. The saturation state of the solution is calculated with respect to an extensive database that identifies solid phases that are thermodynamically stable (candidates for possible precipitation) under relevant conditions (temperature, pH, Eh, oxygen partial pressure, etc.). The aqueous speciation of the solution is also described, as this information can be used to predict the chemical evolution of the system (pH, Eh, saturation state, etc.) if conditions change (temperature, solution composition, etc.). The key observations made in this study are:

- The solution is predicted to be saturated with respect to several solid phases, although some of these are not expected to form due to slow precipitation kinetics. Examples of phases that could form but have unknown precipitation kinetics that may need to be investigated experimentally are ZrO_2 , SnO_2 , BaSO_4 , CoWO_4 , and RuO_2 .
- Uranyl peroxide (studtite or metastudtite) may precipitate if the steady-state concentration of radiolytically generated peroxide is maintained above a certain threshold value. Based on the limited thermodynamic data available, the threshold concentration of hydrogen peroxide for precipitation of uranyl peroxide was found to be around $3.0\text{E-}4$ mol/L at room temperature.
- At temperatures above 50°C up to 100°C the target solution is actually more likely to precipitate ferric iron oxides and a beryllium oxide due to the increasing saturation indices for the system of interest.

3 METHODS

The thermodynamic calculations were done using the Geochemist's Workbench®, Professional Release 8.0 (GWB). The thermodynamic database used was an adapted version of the database "thermo.com.V8.R6.full" [Wolery and Daveler, 1992], which was updated for these calculations using recent literature.

The GWB code uses a Gibb's free energy minimization technique to determine the equilibrium state of the system of interest. Specifically, the code uses equilibrium constants for a set of basis reactions to solve a matrix of mass-balance and charge-balance equations. Results from these calculations feed into an iterative algorithm that converges on a unique equilibrium state for the multi-component, multi-phase system of interest. The code first calculates the aqueous speciation of the solution and then, based on those results, determines whether the solution is saturated with respect to any solid phases by comparing the activity product to the solubility product of each phase.

The GWB code can calculate the activities of electrolyte species ($a_i = \gamma_i m_i$, where a = activity, γ activity coefficient, and m = molal concentration for species i) using a variety of methods [Bethke, 2009]. The two most commonly used methods are (1) the "B-dot" equation, which is an extended form of the Debye-Hückel equation, and (2) the Harvie-Møller-Weare (HMW) implementation of the Pitzer equations. For this report the B-dot method is used because it has been shown to be applicable to solutions of the type in question (multi-component with moderate ionic strength).

Starting with a given solution composition (referred to as the system's basis or list of components) and the assumed constant temperature and pressure, the code first uses a Gibb's free energy minimization technique to determine the concentrations of all chemical species that simultaneously satisfy mass action, mass balance, and charge balance equations for all possible chemical reactions in the system. The point of minimum free energy for an individual chemical reaction is quantified by its equilibrium constant. The thermodynamic database used for calculating the speciation and saturation state of the target solution is essentially a matrix of several thousand equilibrium constants taken from accepted literature sources.

3.1 BUILDING THE THERMODYNAMIC DATABASE

The incorporation of constants into the thermodynamic database used by the GWB code required four steps:

1. Tabulating the free energies of formation (G°_f) for species of interest as well as auxiliary species that are used to write the basis reactions.
2. Writing the basis reactions. These reactions are used by the code to solve the matrix of mass and charge balance equations, which feed into the iterative algorithm that converges on a unique equilibrium state.

3. Calculating the free energy of reaction for the basis reactions (ΔG_r°) using the following equation:

$$\Delta G_r^\circ = \sum_i n_i G_{fi}^\circ (\text{products}) - \sum_i n_i G_{fi}^\circ (\text{reactants}) \quad (1)$$

where n_i is the molar coefficient of species i in the reaction, and G_{fi}° is the free energy of formation for that species.

4. Calculating the equilibrium constants (K_{eq}) for the basis reactions using the following relationships:

$$\Delta G_r^\circ = -RT \ln K_{eq} \quad (2)$$

Since the code uses $\log_{10} K_{eq}$ in its algorithms, the equation actually used is:

$$\log_{10} K_{eq} = -\frac{\Delta G_r^\circ}{2.303RT} \quad (3)$$

where $K_{eq} = [A]^a[B]^b/[C]^c[D]^d$ for the reaction $aA + bB + \leftrightarrow cC + dD$, R is the gas constant, and T is absolute temperature.

The solution saturation state is presented in terms of the saturation index (SI):

$$SI = \log_{10} \frac{Q}{K_{sp}} \quad (4)$$

where Q is the reaction quotient defined as $Q = [A]^a[B]^b/[A_aB_b]$ for the reaction $aA + bB + \leftrightarrow A_aB_b$, and K_{sp} is the equilibrium constant for the precipitation/dissolution reaction in question. The reaction quotient changes continuously during the reaction until equilibrium is achieved and is related to the change in the Gibbs free energy of reaction as follows:

$$\Delta G_r = \Delta G_r^\circ + RT \ln Q \quad (5)$$

Therefore,

$$\log_{10} Q = \frac{\Delta G_r - \Delta G_r^\circ}{2.303RT} \quad (6)$$

At equilibrium, ΔG_r goes to zero and, therefore, $Q = K_{sp}$. Equation 6 can thus be written as

$$\log_{10} K_{sp} = -\frac{\Delta G_r^\circ}{2.303RT} \quad (7)$$

Therefore, at equilibrium, $SI = 0$, the solution is undersaturated if $SI < 0$ and supersaturated if $SI > 0$.

3.2 EXAMPLE OF SATURATION INDEX CALCULATION

For clarity, this example shows the step-by-step arithmetic of the saturation-state calculation for the zirconium-oxide phase baddeleyite (ZrO_2).

The solubility of a mineral is quantified by its solubility product, which is defined as the equilibrium constant (Equations 2–7) for a reaction describing its precipitation and dissolution. For example,



$$k_{ZrO_2} = \frac{(\gamma_{Zr^{4+}})(m_{Zr^{4+}})(\gamma_{H_2O})(m_{H_2O})^2}{(\gamma_{ZrO_2})(m_{ZrO_2})(\gamma_{H^+})(m_{H^+})^4} \quad (9)$$

where k_{ZrO_2} is the solubility product for zirconium oxide, m is the molal concentration for species i , and γ_i is the activity coefficient for species i (calculated using the B-dot Debye-Hückel activity model). Because the activities of water and solid phases equal one for the system of interest:

$$k_{ZrO_2} = \frac{(\gamma_{Zr^{4+}})(m_{Zr^{4+}})}{(\gamma_{H^+})(m_{H^+})^4} \quad (10)$$

When reaction 8 is in equilibrium, $k_{ZrO_2} = 1.147E-08$ at 25°C (thermodynamic data taken from [Robie et al., 1979]). When reaction 8 is not in equilibrium, the following equation (see also Equations 5 and 6) describes the ion activity product or reaction quotient (Q) for the reaction:

$$Q = \frac{(\gamma_{Zr^{4+}})(m_{Zr^{4+}})}{(\gamma_{H^+})(m_{H^+})^4} \quad (11)$$

The saturation index (SI) for a solution is defined as the reaction quotient divided by the solubility product of the mineral phase of interest (Equation 4). Therefore, if $SI = 1$, the solution is saturated with the mineral in question; if $SI > 1$, the solution is supersaturated (metastable); and if $SI < 1$, the solution is undersaturated.

For the zirconium-oxide example, the code, using the B-dot Debye-Hückel activity model and the starting concentrations given in Table 1, calculates:

$$SI = \frac{\frac{(9.0 \times 10^{-4})(1.1 \times 10^{-4})}{[(8.1 \times 10^{-1})(9.9 \times 10^{-2})]^4}}{1.147E-08} = \frac{2.4 \times 10^{-3}}{1.147 \times 10^{-8}} = 2.1 \times 10^5 \quad (12)$$

This result indicates that the solution described in Table 1 is supersaturated with respect to the mineral baddeleyite (ZrO_2), that is, there is a thermodynamic driving force for this mineral to precipitate. However, as is commonly observed, kinetic energy barriers related to nucleation and crystal growth (bond formation) might keep the solution in a meta-stable state (no precipitation) under certain conditions.

3.3 SPECIATION/SATURATION STATE OF IRRADIATED SHINE SOLUTION

The following section discusses a speciation/saturation state calculation for an irradiated uranyl sulfate solution with a composition determined by ORIGEN calculations [Driscoll, 2014]. The assumptions used for this calculation are as follows:

- The temperature was constant at 25°C.
- The pH was varied for speciation calculations over a range of 0 to 2.
- Electroneutrality of the solution was maintained by addition or subtraction of SO_4^{--} (using a titration model) over model pH range.
- The target solution composition reflected
 - No UREX processing prior to fuel preparation (the solution contains the original uranium impurities)
 - Irradiation periods of 5.5 days
 - Power in target solution of 137.5 kWt (10% above 125 kWt licensed power limit)
 - 6-hour decay prior to molybdenum extraction
 - 97% of molybdenum extracted
 - 90% of selenium and tellurium extracted
 - 97% of zirconium extracted
 - 5.8-hour decay after extraction, before start of subsequent cycle

4 DISCUSSION

4.1 SPECIATION AND SATURATION CALCULATIONS AT ROOM TEMPERATURE

Table 1 shows the starting composition of the target solution used in the thermodynamic calculations. Since the objective was to evaluate for possible precipitation, the maximum concentration of each element attained during a four-cycle run was used. The concentrations of key elements in the target solution over the four-cycle run are shown in Figure 1. The top figure shows elements that are removed after each cycle, and the bottom figure shows elements that accumulate over the duration of four cycles.

The equilibrium chemical distribution of elements (speciation) within the simulated target solution (Table 1) is shown in Table 2. The aqueous speciation at the 25°C equilibrium pH and oxidation/reduction potential (Eh) is shown, as well as the saturation indices of stable solids. The amounts of some of the solids thermodynamically predicted to precipitate are also shown.

Figure 2 shows how the saturation indices of key phases vary over the pH range 0 to 2. The aqueous speciation (for selected elements) over this pH range is shown in Figure 3. Figure 4 shows results from a calculation related to the saturation state of uranyl peroxide in the target solution. It indicates that a steady-state hydrogen peroxide concentration greater than $3.0\text{E-}4$ mol/kg is required to precipitate uranium as a peroxide at pH 1.1 (ignoring kinetic limitations). Under the assumed conditions, as much as 25 g of uranyl peroxide may precipitate per kilogram target solution.

4.2 SPECIATION AND SATURATION CALCULATIONS OF TEMPERATURE EFFECT

Figures 5-7 show thermodynamic (GWB) model results for how increasing the temperature of the solution shown in Table 1 influences speciation and mineral saturation for selected elements.

The example of ruthenium speciation is shown (Figure 5) because the model indicates that, above 80°C, this element could be present as an anionic complex that could affect the process for titania anionic column extraction. Higher temperature also favors the formation of I_2 over iodate species (Figure 5).

Uranyl minerals, such as $\text{UO}_2\text{SO}_4 \cdot 2.5\text{H}_2\text{O}$, show “retrograde” solubility (Figure 5); that is, their saturation indices increase with increasing temperature (they are less soluble at higher temperature). The ferric oxides hematite (Fe_2O_3) and goethite (FeOOH) also show retrograde solubility and are predicted to become saturated around 55°C and 75°C, respectively (Figure 6).

The solubility of cassiterite (SnO_2), baddelyite (ZrO_2), barite (BaSO_4), quartz (SiO_2), and CoWO_4 are “prograde,” that is, their solubilities increase with increasing temperature; however, only quartz is predicted to become undersaturated (around 70°C) (Figure 6). The model predicts

TABLE 1 Input Solution Composition for Speciation Modeling

Element	mol/kg-H ₂ O	mg/kg-H ₂ O
Hydrogen	1.112E+02	9.295E+04
Oxygen	5.913E+01	7.844E+05
Sulfur	6.336E-01	1.685E+04
Uranium	5.347E-01	1.055E+05
Carbon	3.699E-03	3.684E+01
Aluminum	7.051E-04	1.578E+01
Iron	5.676E-04	2.629E+01
Silicon	4.516E-04	1.052E+01
Zirconium	3.517E-04	2.661E+01
Calcium	3.153E-04	1.048E+01
Magnesium	2.609E-04	5.259E+00
Nickel	2.160E-04	1.051E+01
Phosphorus	2.047E-04	5.258E+00
Sodium	1.380E-04	2.631E+00
Molybdenum	1.349E-04	1.073E+01
Chromium	1.219E-04	5.256E+00
Tin	1.065E-04	1.048E+01
Copper	9.973E-05	5.255E+00
Vanadium	7.448E-05	3.146E+00
Tungsten	6.893E-05	1.051E+01
Manganese	5.539E-05	2.523E+00
Lithium	3.388E-05	1.950E-01
Beryllium	1.410E-05	1.054E-01
Cobalt	1.076E-05	5.259E-01
Boron	9.413E-06	8.439E-02
Cerium	8.292E-06	9.635E-01
Plutonium	3.828E-06	7.745E-01
Cesium	6.395E-06	7.048E-01
Barium	5.417E-06	6.169E-01
Strontium	5.189E-06	3.770E-01
Ruthenium	4.981E-06	4.175E-01
Dysprosium	3.806E-06	5.129E-01
Neodymium	3.637E-06	4.350E-01
Lanthanum	3.407E-06	3.924E-01
Lead	3.020E-06	5.189E-01
Yttrium	2.684E-06	1.979E-01
Praseodymium	1.741E-06	2.034E-01
Europium	1.738E-06	2.190E-01
Samarium	1.721E-06	2.146E-01
Selenium	4.793E-08	3.138E-03
Iodine	9.965E-09	1.049E-03

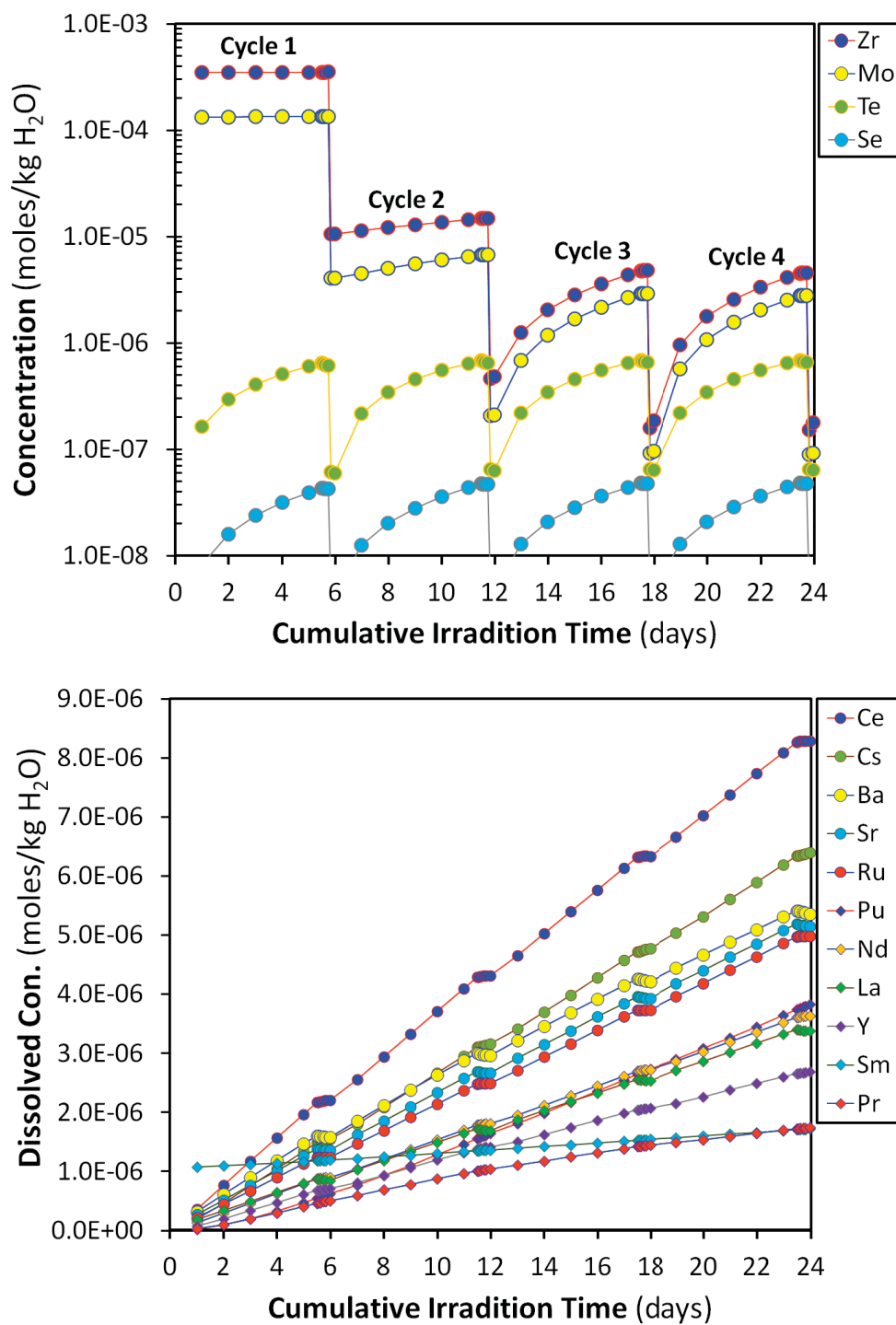


FIGURE 1 Concentrations of Key Elements in the Target Solution over a Four-Cycle Run. The maximum concentration of each element was used for the thermodynamic calculations. For elements shown in the top figure, this occurs after the first cycle (505 days); for elements in the bottom figure, this occurs at the end of the fourth cycle (24 hours).

TABLE 2 Speciation and Saturation State of Solution Composition Shown in Table 1

Temperature (°C)	25.0	pH	1.1
Pressure (bar)	1.013	Eh (volts)	1.125
Solution mass (kg)	1.206	O ₂ (g)	0.002
Solution density (kg/L)	1.101	CO ₂ (g)	0.109
Mineral Saturation States (log₁₀Q/K)			
<i>Saturated</i>		<i>Undersaturated</i>	
*Ba ₃ PuO ₆	51.677	MoO ₃	-0.278
*Ba ₂ SrPuO ₆	48.016	PbSO ₄	-0.500
*Sr ₃ PuO ₆	46.614	SiO ₂ (amorphous)	-0.632
ZrO ₂	5.328	(UO ₂) ₃ (PO ₄) ₂ ·4H ₂ O	-1.311
SnO ₂	3.567	UO ₂ HPO ₄ ·4H ₂ O	-1.473
Pb(UO ₂) ₂ (PO ₄) ₂ ·10H ₂ O	2.045	FeO(OH)	-1.622
*UO ₂ SO ₄ ·H ₂ O	2.380	UO ₂ HPO ₄	-1.817
BaSO ₄	1.918	CaSO ₄ ·2H ₂ O	-1.827
CoWO ₄	1.827	CaSO ₄	-2.003
RuO ₂	1.599	Fe ₂ O ₃	-2.284
*BaPuO ₃	0.763	H _{0.33} Fe ₂ Al _{0.33} Si _{3.67} H ₂ O ₁₂	-2.363
*SiO ₂ (cr)	0.654	(UO ₂) ₂ SiO ₄ ·2H ₂ O	-2.446
#H ₂ MoO ₄ (cr)	0.122	SrSO ₄	-2.517
Predicted Amounts of Selected Precipitates (mg)			
ZrO ₂	43.339		
SnO ₂	16.047		
BaSO ₄	1.249		
CoWO ₄	3.243		
RuO ₂	0.646		
Aqueous Species (mol/L)			
UO ₂ SO ₄ (aq)	2.945E-01	H ₂ SO ₄ (aq)	5.398E-06
UO ₂ ⁺⁺	1.703E-01	Ru(OH) ₂ ⁺⁺	5.023E-06
UO ₂ (SO ₄) ₂ ⁻⁻	1.219E-01	Sr ⁺⁺	4.308E-06
H ⁺	1.085E-01	UO ₂ OH ⁺	3.599E-06
HSO ₄ ⁻	1.019E-01	Pb ⁺⁺	3.325E-06
SO ₄ ⁻⁻	5.600E-02	NdSO ₄ ⁺	3.263E-06
CO ₂ (aq)	4.073E-03	O ₂ (aq)	3.085E-06
(UO ₂) ₂ OH ⁺⁺⁺	8.614E-04	LaSO ₄ ⁺	2.569E-06
Fe ⁺⁺⁺	5.501E-04	DySO ₄ ⁺	2.158E-06
SiO ₂ (aq)	4.972E-04	PuO ₂ SO ₄ (aq)	2.111E-06
AlSO ₄ ⁺	2.977E-04	H ₃ PO ₄ (aq)	1.886E-06
Al ⁺⁺⁺	2.901E-04	LiSO ₄ ⁻	1.878E-06
Ca ⁺⁺	2.773E-04	YSO ₄ ⁺	1.786E-06
UO ₂ H ₂ PO ₄ ⁺	1.969E-04	(UO ₂) ₂ (OH) ₂ ⁺⁺	1.747E-06
Ni ⁺⁺	1.887E-04	Dy ⁺⁺⁺	1.633E-06
Al(SO ₄) ₂ ⁻	1.884E-04	PuO ₂ (SO ₄) ₂ ⁻⁻	1.504E-06
Mg ⁺⁺	1.738E-04	SrSO ₄ (aq)	1.404E-06
Na ⁺	1.441E-04	SnOH ⁺⁺⁺	1.271E-06
Cr ⁺⁺⁺	1.338E-04	SmSO ₄ ⁺	1.245E-06

TABLE 2 (Cont.)

Zr ⁺⁺⁺⁺	1.245E-04	Pr ⁺⁺⁺	1.162E-06
MgSO ₄ (aq)	1.133E-04	UO ₂ HPO ₄ (aq)	9.683E-07
Sn(OH) ₄ (aq)	1.096E-04	EuSO ₄ ⁺	8.307E-07
Zr(OH) ₄ (aq)	9.181E-05	Pr(SO ₄) ₂ ⁻	7.546E-07
H ₂ MoO ₄ (aq)	8.013E-05	Nd ⁺⁺⁺	7.404E-07
Cu ⁺⁺	7.592E-05	Y ⁺⁺⁺	7.088E-07
WO ₄ ⁻	7.588E-05	Eu ⁺⁺⁺	6.286E-07
CaSO ₄ (aq)	6.975E-05	MoO ₂ (H ₂ O) ₄ ⁺⁺	6.198E-07
Zr(OH) ₃ ⁺	6.859E-05	La(SO ₄) ₂ ⁻	5.998E-07
VO ₂ ⁺	6.237E-05	PuO ₂ ⁺⁺	5.983E-07
ZrOH ⁺⁺⁺	6.087E-05	La ⁺⁺⁺	5.826E-07
NiSO ₄ (aq)	4.907E-05	Y(SO ₄) ₂ ⁻	4.603E-07
FeSO ₄ ⁺	4.668E-05	Ru(OH) ₂ SO ₄ (aq)	4.600E-07
Mn ⁺⁺	4.238E-05	Eu(SO ₄) ₂ ⁻	4.541E-07
Li ⁺	3.542E-05	Dy(SO ₄) ₂ ⁻	4.002E-07
CuSO ₄ (aq)	3.387E-05	Sm(SO ₄) ₂ ⁻	3.663E-07
MoO ₂ (OH)(H ₂ O) ₃ ⁺	3.355E-05	HCrO ₄ ⁻	3.648E-07
MoO ₃ (H ₂ O) ₃ (aq)	2.593E-05	Sn(OH) ₂ ⁺⁺	3.495E-07
UO ₂ H ₃ PO ₄ ⁺⁺	2.522E-05	Sm ⁺⁺⁺	2.826E-07
FeOH ⁺⁺	2.032E-05	VO(OH) ₃ (aq)	2.624E-07
ZrSO ₄ ⁺⁺	1.954E-05	Mo ₂ O ₅ (H ₂ O) ₆ ⁺⁺	2.422E-07
VO ₂ SO ₄ ⁻	1.933E-05	H ₂ PO ₄ ⁻	2.409E-07
MnSO ₄ (aq)	1.860E-05	Mo ₂ O ₅ (OH)(H ₂ O) ₅ ⁺	1.852E-07
Be ⁺⁺	1.552E-05	Fe ₂ (OH) ₂ ⁺⁺⁺⁺	1.737E-07
Zr(SO ₄) ₂ (aq)	1.408E-05	Zr ₃ (OH) ₄ ⁺⁺⁺⁺⁺⁺	1.702E-07
Co ⁺⁺	1.182E-05	HMoO ₄ ⁻	1.431E-07
B(OH) ₃ (aq)	1.036E-05	FeHPO ₄ ⁺	1.173E-07
Ce ⁺⁺⁺	9.128E-06	CrOH ⁺⁺	7.653E-08
NaSO ₄ ⁻	7.765E-06	Mo ₂ O ₄ (OH)(H ₂ O) ₆ ⁺	3.759E-08
Fe(SO ₄) ₂ ⁻	7.356E-06	HCO ₃ ⁻	3.477E-08
Zr(SO ₄) ₃ ⁻	7.234E-06	HSeO ₄ ⁻	3.193E-08
MoO ₂ ⁺⁺	7.203E-06	Sn ⁺⁺⁺⁺	2.961E-08
Cs ⁺	7.040E-06	CoSO ₄ (aq)	2.544E-08
Sn(OH) ₃ ⁺	6.037E-06	Fe(OH) ₂ ⁺	2.292E-08
Ba ⁺⁺	5.963E-06	SeO ₄ ⁻	2.076E-08

* Denotes kinetically unfavorable phase (not predicted to precipitate at 25°C).

Denotes significant uncertainty in solubility product.

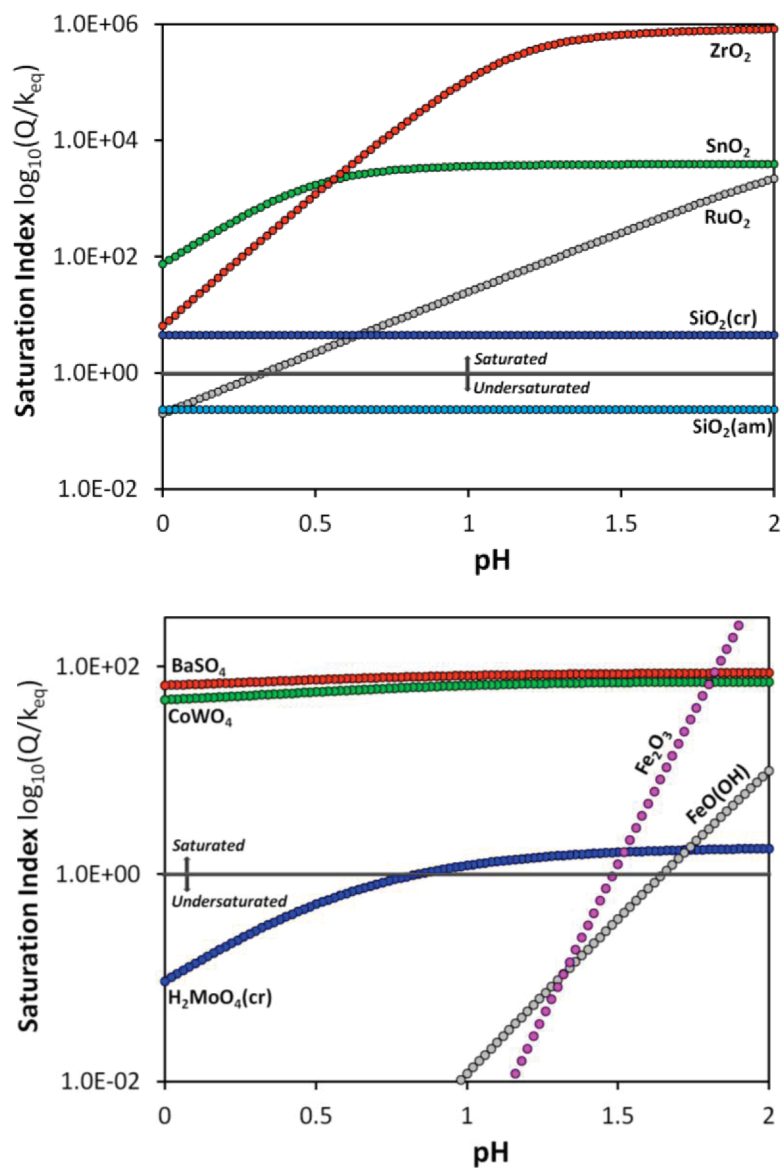


FIGURE 2 Variation of Saturation Indices with pH for the Target Solution Composition Shown in Table 1 (constant temperature = 25°C)

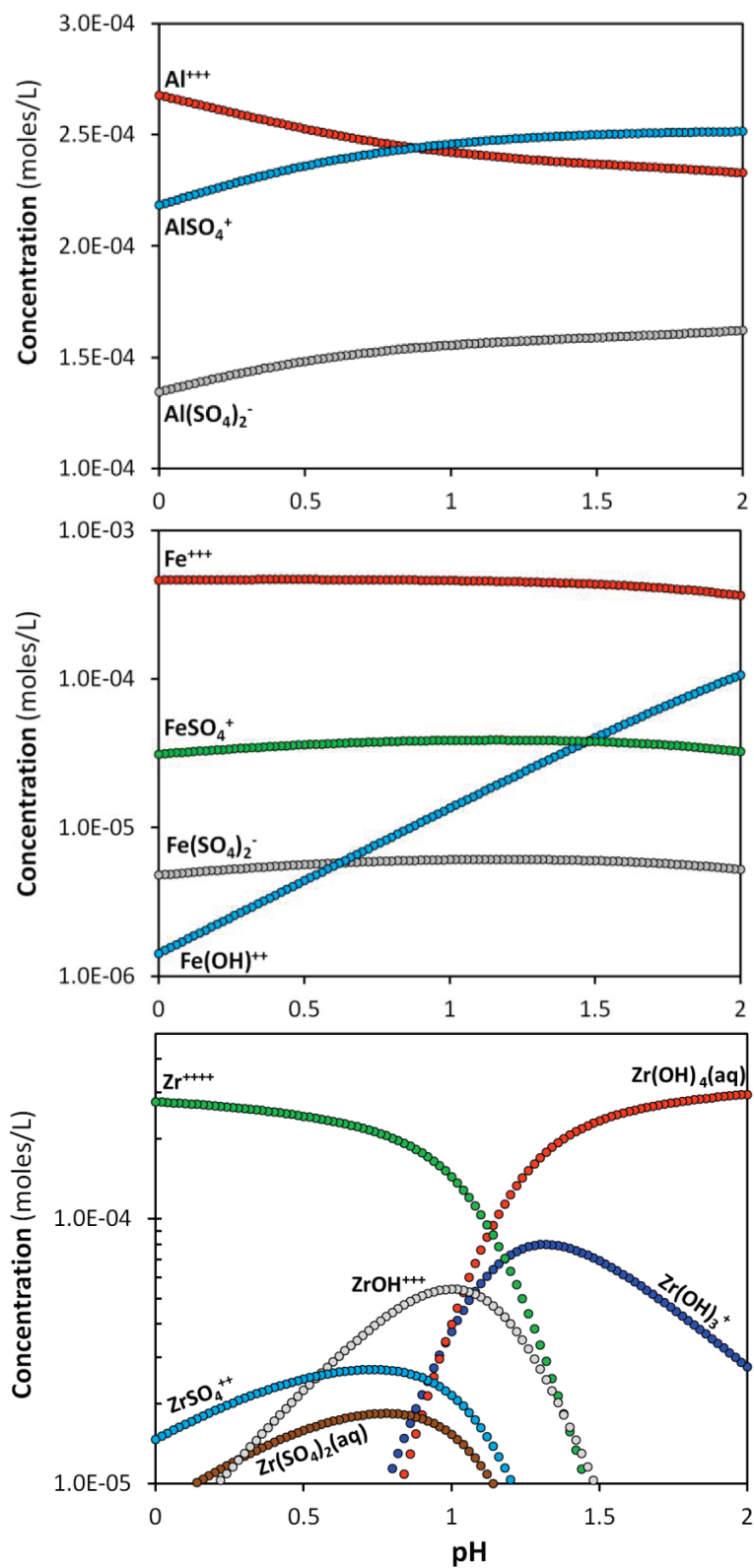


FIGURE 3 Variation of Aqueous Speciation with pH for the Target Solution Composition Shown in Table 1 (constant temperature = 25°C)

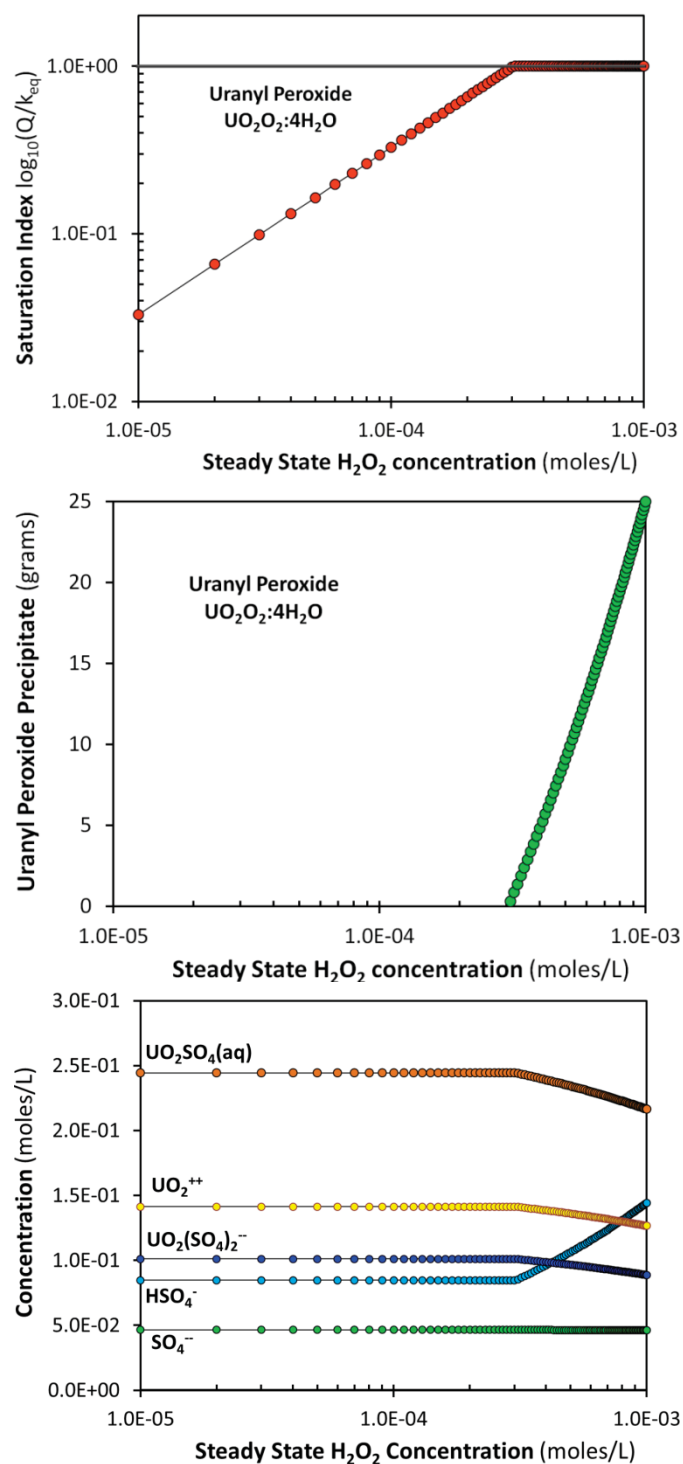


FIGURE 4 Saturation Index and Selected Speciation of Target Solution over a Range of Steady-State Concentrations of Dissolved Hydrogen Peroxide. Uranium is predicted to precipitate as uranyl peroxide if the concentration of hydrogen peroxide exceeds $3.0\text{E-}4$ mol/L. About 25 grams of uranyl peroxide may precipitate in a liter of target solution under these conditions.

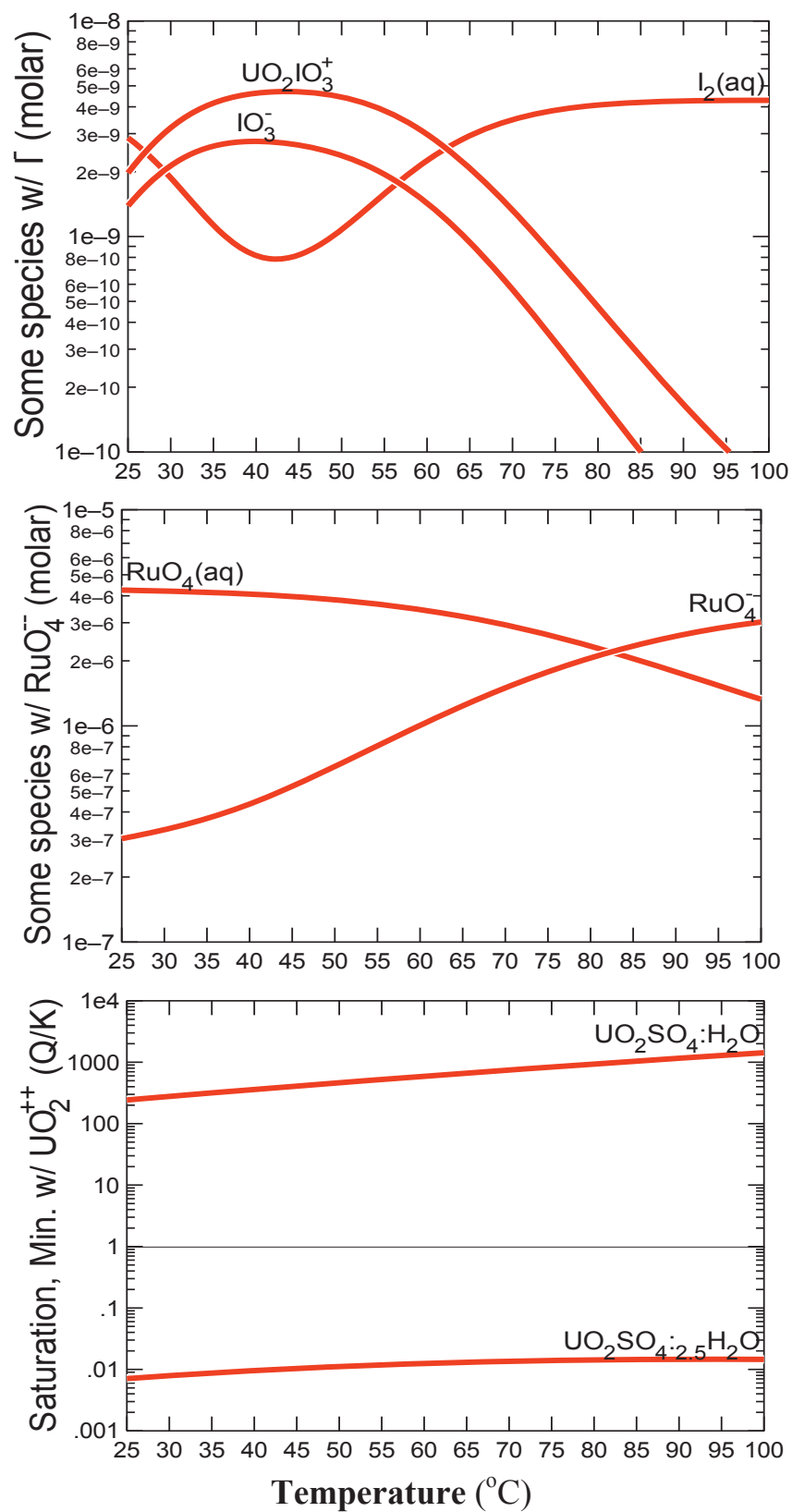


FIGURE 5 Selected Examples of How Saturation Indices and Key Species Change over the Temperature Range 25°C to 100°C

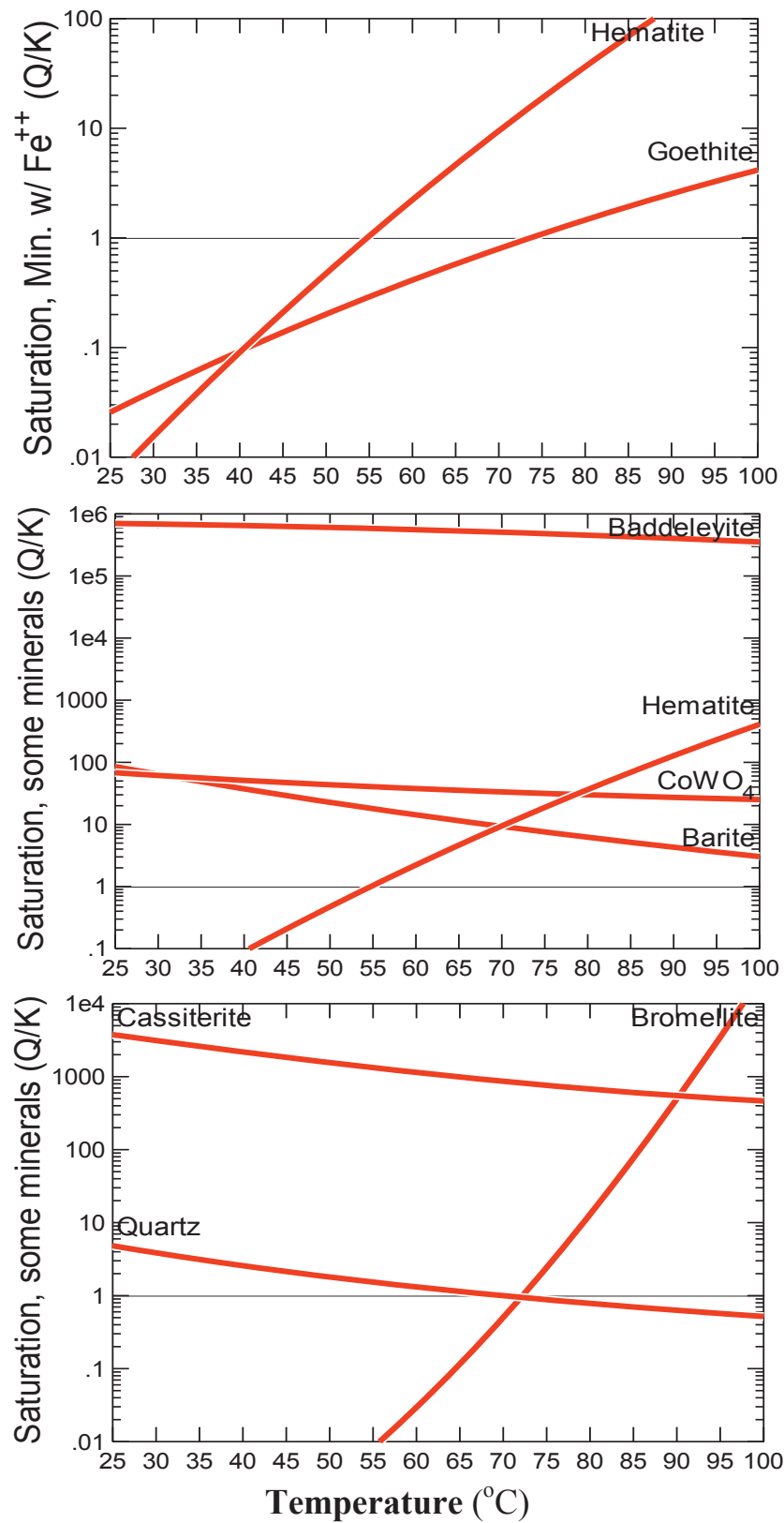


FIGURE 6 Additional Examples of How Saturation Indices and Key Species Change over the Temperature Range 25°C to 100°C

that beryllium may precipitate as bromellite (BeO) at elevated temperatures (above 70°C). The solubility of bromellite is predicted to decrease dramatically with increasing temperature; however, few experimental data are available on this phase, and more data are needed to fully assess its importance.

4.3 REDUCTION/OXIDATION (REDOX) RELATIONSHIPS BETWEEN KEY SPECIES

The equilibrium redox speciation is presented below in terms of Eh, which is defined as the electromotive force (emf) generated between an electrode in any state and the hydrogen electrode ($\text{H}_2(\text{g}) \rightarrow 2\text{H}^+ + 2\text{e}^-$) in the standard state. The hydrogen electrode in the standard state has a standard potential or standard emf (E°) of zero. The emf is the electrical potential generated by a redox half-reaction. Eh is calculated using the following relationships (for the half-reaction $a\text{A} + b\text{B} + n\text{e}^- \leftrightarrow c\text{C} + d\text{D}$):

$$E_h = E^\circ + \frac{RT}{nF} \ln \frac{(A)^a (B)^b}{(C)^c (D)^d} \quad (13)$$

which is equivalent to:

$$E_h = E^\circ + 2.303 \frac{RT}{nF} \log_{10} K_{eq} \quad (14)$$

where n is the number of electrons transferred during the half-reaction, and F is the Faraday constant. The standard potential (E°) is related to the change in the Gibbs free energy of formation and $\log_{10} K_{eq}$ for the half-reaction, as follows:

$$E^\circ = \frac{\Delta G_r^\circ}{nF} \quad (15)$$

Substituting Eq. 7 into Eq. 15 yields

$$E^\circ = -\frac{2.303RT}{nF} \log_{10} K_{eq} \quad (16)$$

Figures 7 – 9 show that, if the redox state of the Table 1 solution (pH = 1) were to decrease (e.g., due to consumption of dissolved oxygen and/or the oxidation of radiolytic hydrogen), the order in which some key redox species would be reduced is as follows:

- At Eh = 0.9 volts, V(V) reduces to V(IV).
- At Eh = 0.8 volts, I₂ reduces to iodide.

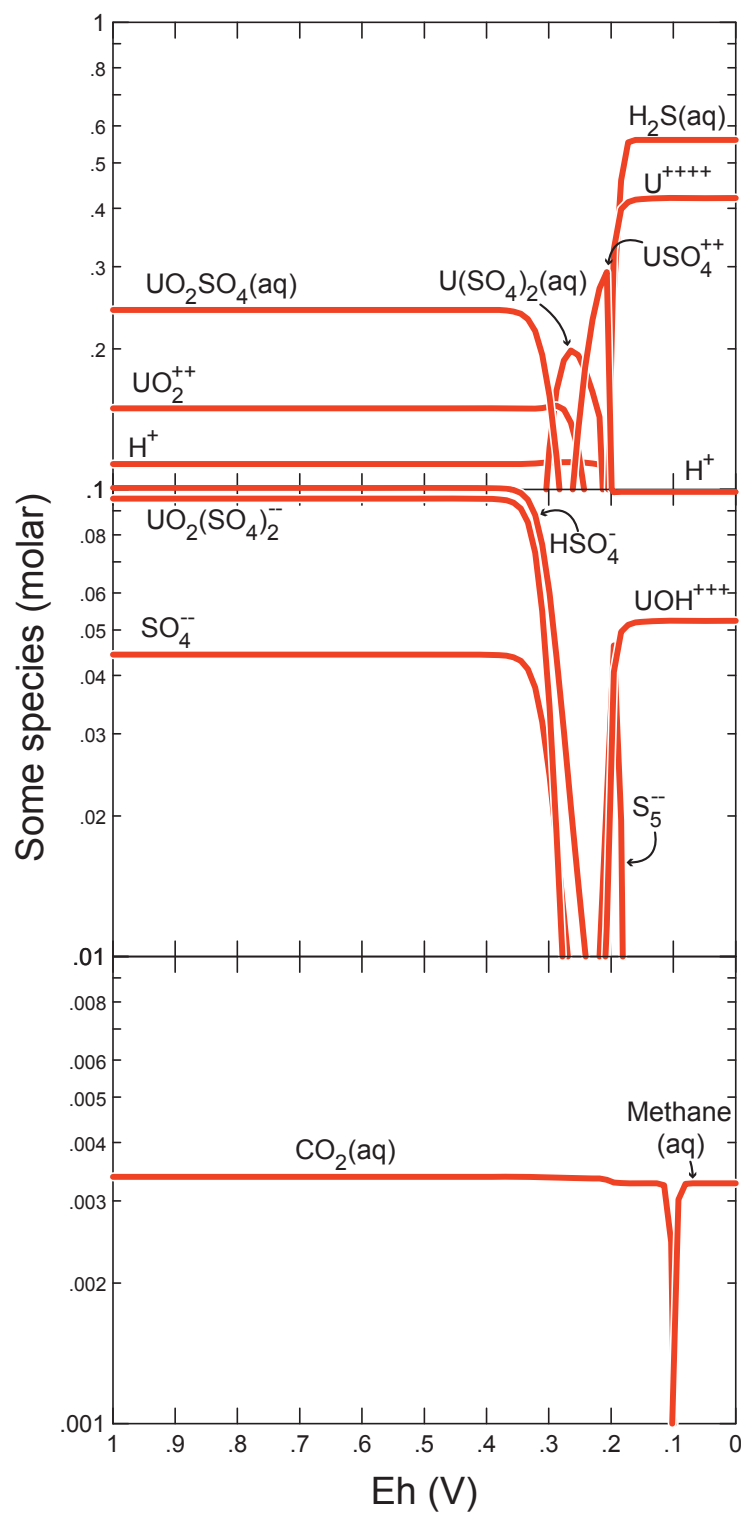


FIGURE 7 First Example of Redox Relationships between Selected Species from Table 2. The plots show how concentrations of key species vary as the redox conditions of the solution are varied from 1 volt down to zero volts at pH = 1.

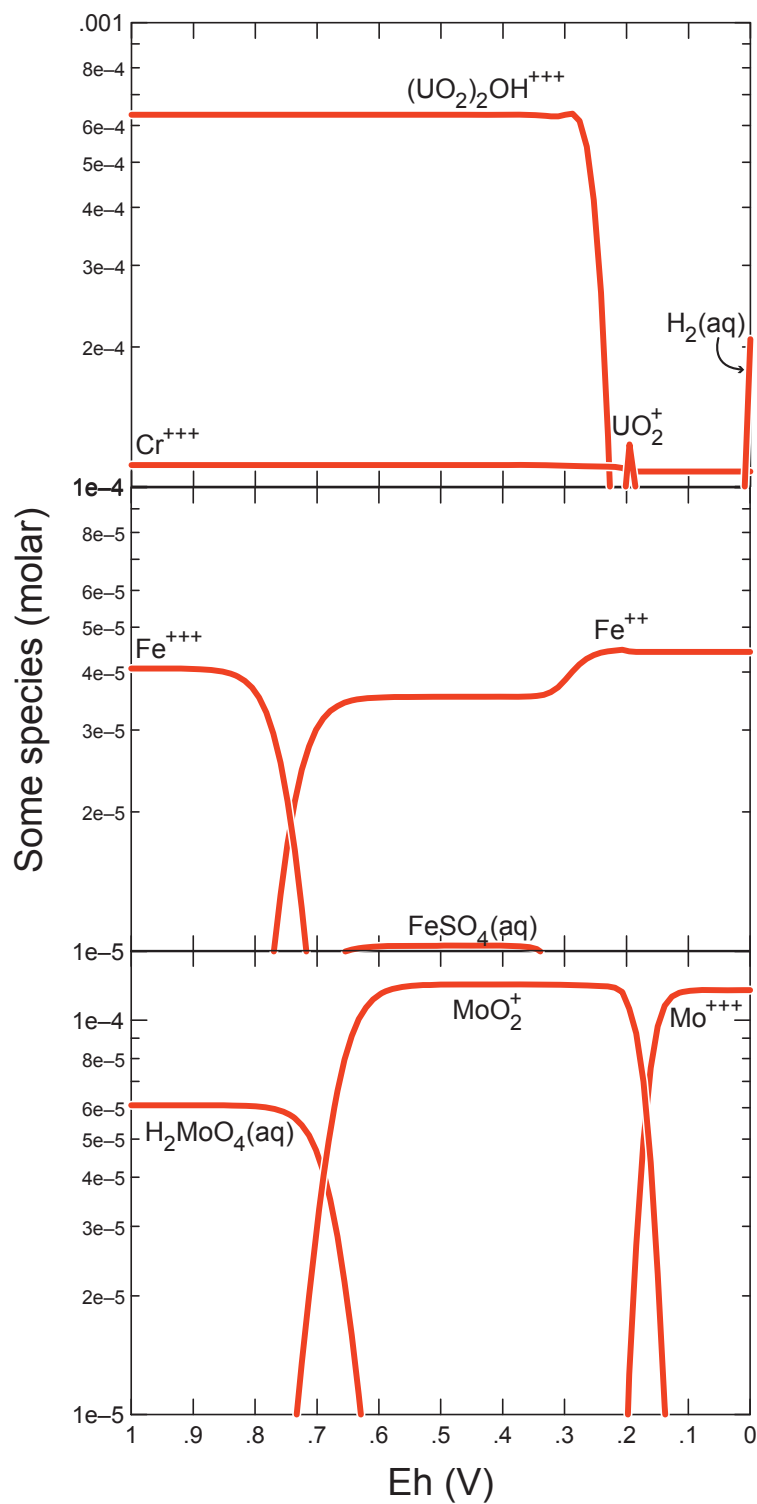


FIGURE 8 Second Example of Redox Relationships between Selected Species from Table 2. The plots show how concentrations of key species vary as the redox conditions of the solution are varied from 1 volt down to zero volts at pH = 1.

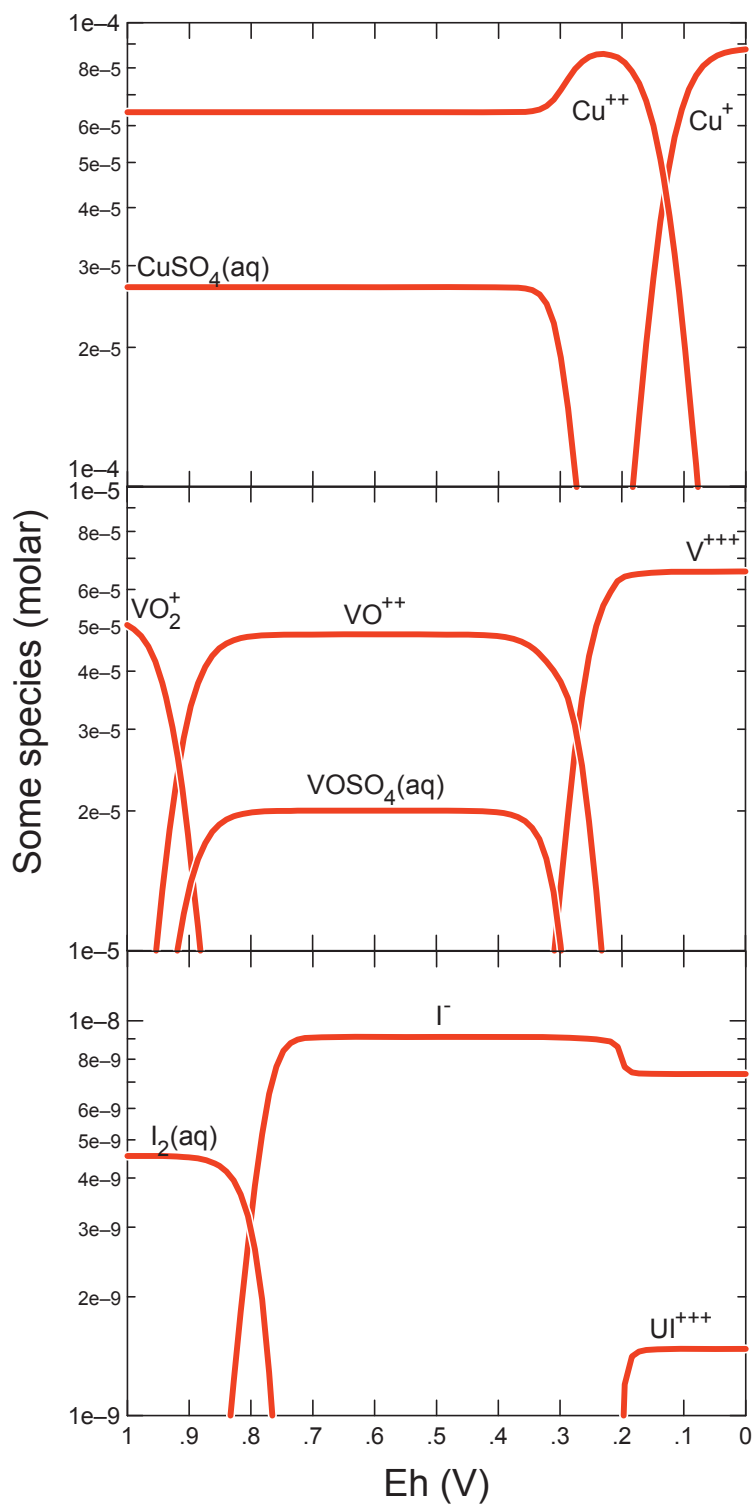


FIGURE 9 Third Example of Redox Relationships between Selected Species from Table 2. The plots show how concentrations of key species vary as the redox conditions of the solution are varied from 1 volt down to zero volts at pH = 1.

- At Eh = 0.75 volts, Fe(III) reduces to Fe(II).
- At Eh = 0.7 volts, Mo(VI) reduces to Mo(V).
- At Eh = 0.3 volts, U(VI) reduces to U(IV) and V(IV) goes to V(III).
- Below Eh = 0.2 volts, S(VI) reduces to S(-II), Mo(IV) goes to Mo(III), Cu(II) goes to Cu(I), and CO₂ reduces to methane.

4.4 CHEMICAL EFFECTS OF STEEL CORROSION

Previous work with solution reactors can provide important insights that can be used to optimize the SHINE process. For example, the following quotes, extracted from a declassified report from Oak Ridge National Laboratory [Swartout et al., 1953], underscore the importance of having a predictive understanding of steel corrosion and actinide/fission product precipitation:

Corrosion data [on 300 series steels] were accumulated during two natural-uranium runs made prior to the power operation. The initial corrosion rate during these runs was about 9 mpy [mils per year, equivalent to around 5 g/m²day] and steadily decreased to a rate of 1 to 2 mpy [0.5 – 1.0 g/m²day] at the end of 85 hr of operation at 200°C. In the enriched uranium runs, a similar decrease in the corrosion rate was experienced. For the first 20 hr at 200°C and 100 kw, the rate was 40 mpy [22 g/m²day]. Following this period, the reactor dump line was found to be plugged, although the plug apparently dissolved or decomposed after three days. Later, during an operating period of 67 hr at 200°C and a power level of 500 to 1000 kw, the general corrosion rate for the system was measured at about 3 mpy [1.7 g/m²day]. (page v)

The plugging of the dump line may have been caused by uranium peroxide from the sampler, hydrolytically precipitated uranium trioxide, corrosion scale broken loose by the earlier hot dump, or corrosion products and uranium dioxide possibly produced in the normally stagnant dump line where the solution is depleted of oxygen. The evidence is not sufficient for distinguishing between these possibilities for plugging the dump line, and, of course, more than one effect may have occurred at the same time. (page 4)

After the dump line was unplugged, the reactor was again taken critical at 100°C on September 19, 1953, and it was operated at a power level which later proved to be 70 kw to permit measurements for fuel inventory purposes. A voluminous gray precipitate, which proved to be 70% uranium peroxide and 30% Fe, Cr, and Ni oxides, was observed in a fuel sample. Another sample taken after 2 hr of operation at 100 to 120°C and zero power indicated that the uranium peroxide precipitate had been decomposed satisfactorily. (page 4)

The modeling studies being performed for this task will inform experiments designed to further elucidate the corrosion and precipitation processes observed in previous solution reactor tests.

The specific purpose of these model runs is to determine the effect that steel corrosion could have on the chemistry of the SHINE solution. The model tracks the equilibrium speciation of the solution, including saturation indices, as the components of 316 stainless steel are “titrated” into the system (simulating corrosion of pipes and tanks). The composition of the SHINE solution used is given in Table 1, and the composition of the stainless steel used is given in Table 3.

A cursory literature search revealed that the corrosion rates for 300 series stainless steels in uranyl sulfate and other acidic metal sulfate solutions are strongly temperature dependent and generally range from 0.01 to 1.0 g/m²•days at temperatures less than 150°C (Figure 10) [Swartout et al., 1953]. Based on this and other previous work, it seems reasonable to use steel corrosion rates in the range of 0.01 to 1.0 g/m²•days for our model; however, the steel surface area contacted by the solution depends on specific design information that is unavailable at this time. The amount of steel components added to the solution, which is what this modeling effort specifically deals with, also varies with the flow rate or residence time of a given volume of solution within a given steel pipe or tank. This dynamic system aspect is not dealt with in this study but will be accounted for in future model runs.

Varying the steel corrosion rate between 0.1 and 1.0 g/m²•day and the corroding surface area to solution volume ratio between 0.1 and 0.5 m²/L results in a total amount of steel corroded from 0.3 to 15 g over an arbitrarily chosen time period of 30 days (Figure 11). Based on this cursory analysis of previous work our speciation model assumes the reaction of 5 g of steel (Table 3), with the SHINE solution (Table 1). Results given here are preliminary and are only meant to show the general evolution of the chemical system during steel corrosion. Ongoing experimental and modeling work will put the corrosion rates used in Figure 11 in perspective.

The dissolved concentration of oxygen is assumed to be fixed by an O₂ fugacity of 1.0E-6. This assumption results in a constant Eh of around 1 V, at which U(VI), S(VI), and Fe(III) are the dominant redox states. If the O₂ concentration is not fixed for the steel corrosion model, the Eh drops from around 1 V down to just below 0.4 V with around 200 mg of steel

TABLE 3 Nominal Composition of Stainless Steels (in mass%) Used in Modeling. The model involved “titrating” the steel composition (model input row) into the SHINE solution from Table 1.

Steel Type	Fe	Cr	Ni	Mn	Si	Mo
304	67.0	20.0	10.0	2.0	1.0	----
316	61.0	18.0	15.0	2.0	1.0	3.0
Model input (g)	3.05	0.9	0.75	0.1	0.05	0.15

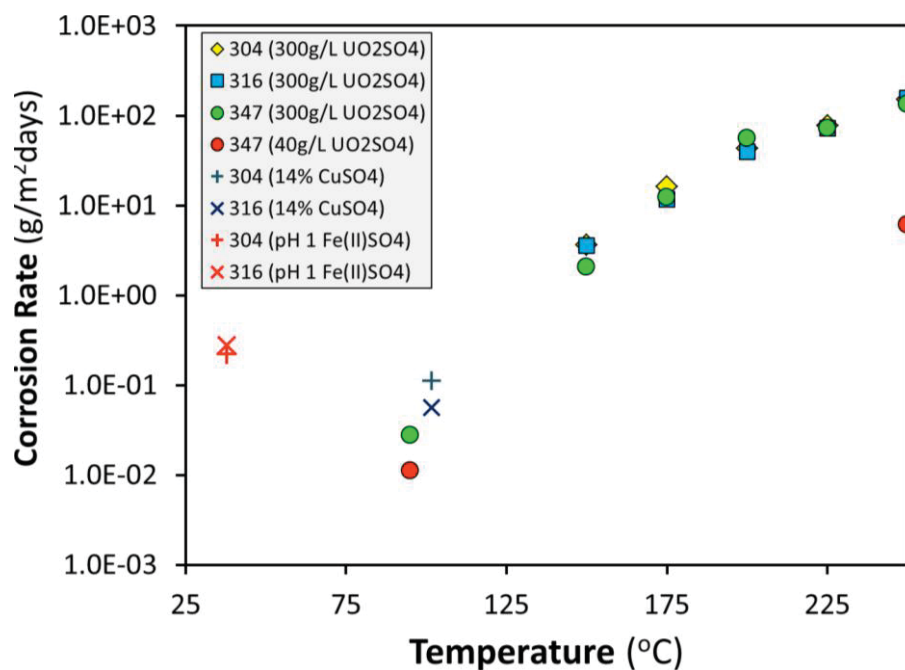


FIGURE 10 Examples of Measured Steel Corrosion rates for 304, 316, 347 Stainless Steels in Uranyl Sulfate, Copper Sulfate, and Ferrous Sulfate Solutions at Different Temperatures (Swartout et al., 1953)

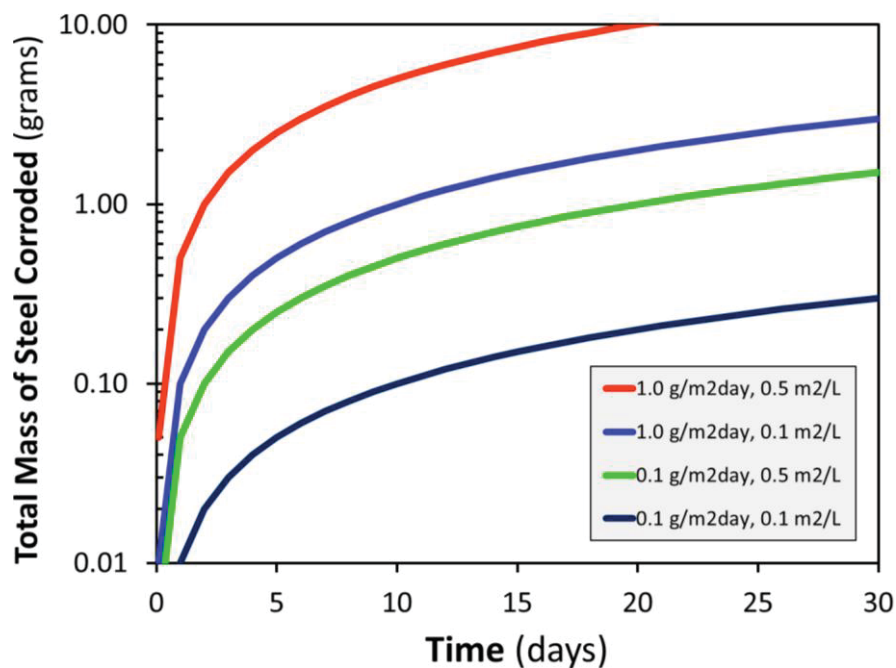


FIGURE 11 Amount of Steel Corroded per Time Given Relevant Ranges of the Corrosion Rate (0.1–1.0 g/m²•day) and Corroding Surface Area per Solution Volume (0.1–0.5 m²/L)

reacted. This is a low enough Eh to reduce the uranyl ion to U(IV) but is deemed unlikely to occur due to the radiolytic production of O₂ in solution.

If it is assumed that the growth of ferric corrosion products is negligible, the pH of the SHINE solution is predicted to increase to just over 2 for a mass of 5 g of steel corroded (Figure 12, plots on left) (see discussion above for why 5 g of steel was chosen). If it is assumed that ferric corrosion products precipitate with no kinetic inhibition, the pH is predicted to increase to around 1.4 for 5 g of steel corrosion (Figure 12, plots on right).

The aqueous speciation of the SHINE solution that corresponds to the model run summarized in Figure 12, left side plots, is shown in Figure 13. The effects of the addition of nonradioactive Cr, Ni, and Mo on the system chemistry are the subject of ongoing modeling studies and will be discussed in the next progress report.

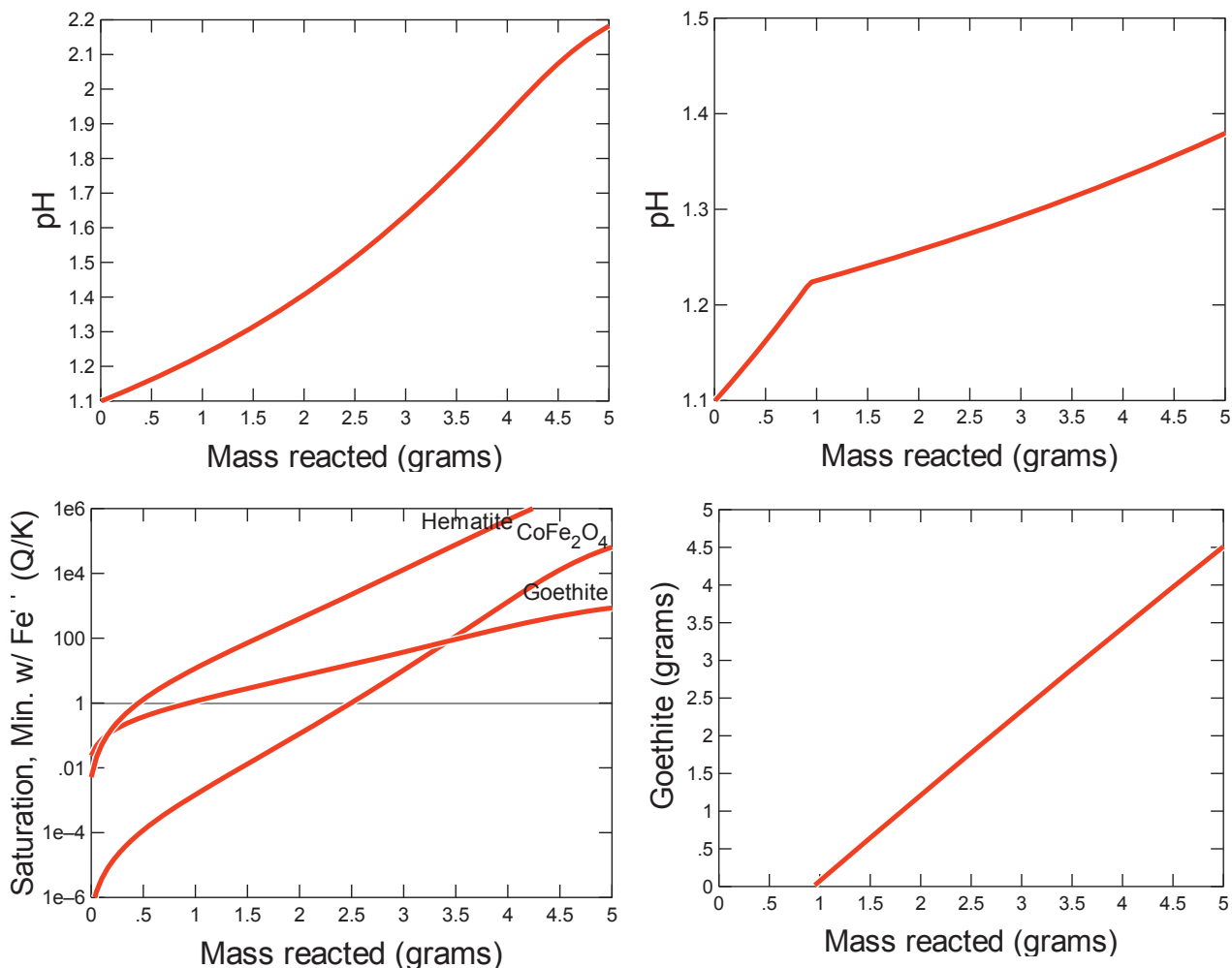


FIGURE 12 Equilibrium Model Results for the Dissolution of 316 Stainless Steel (Table 3) in the SHINE Solution (Table 1). The plots on the left are for a run in which precipitation of iron oxides was suppressed. The plots on the right are for a case where goethite [FeO(OH)] is allowed to precipitate (equilibrate with solution).

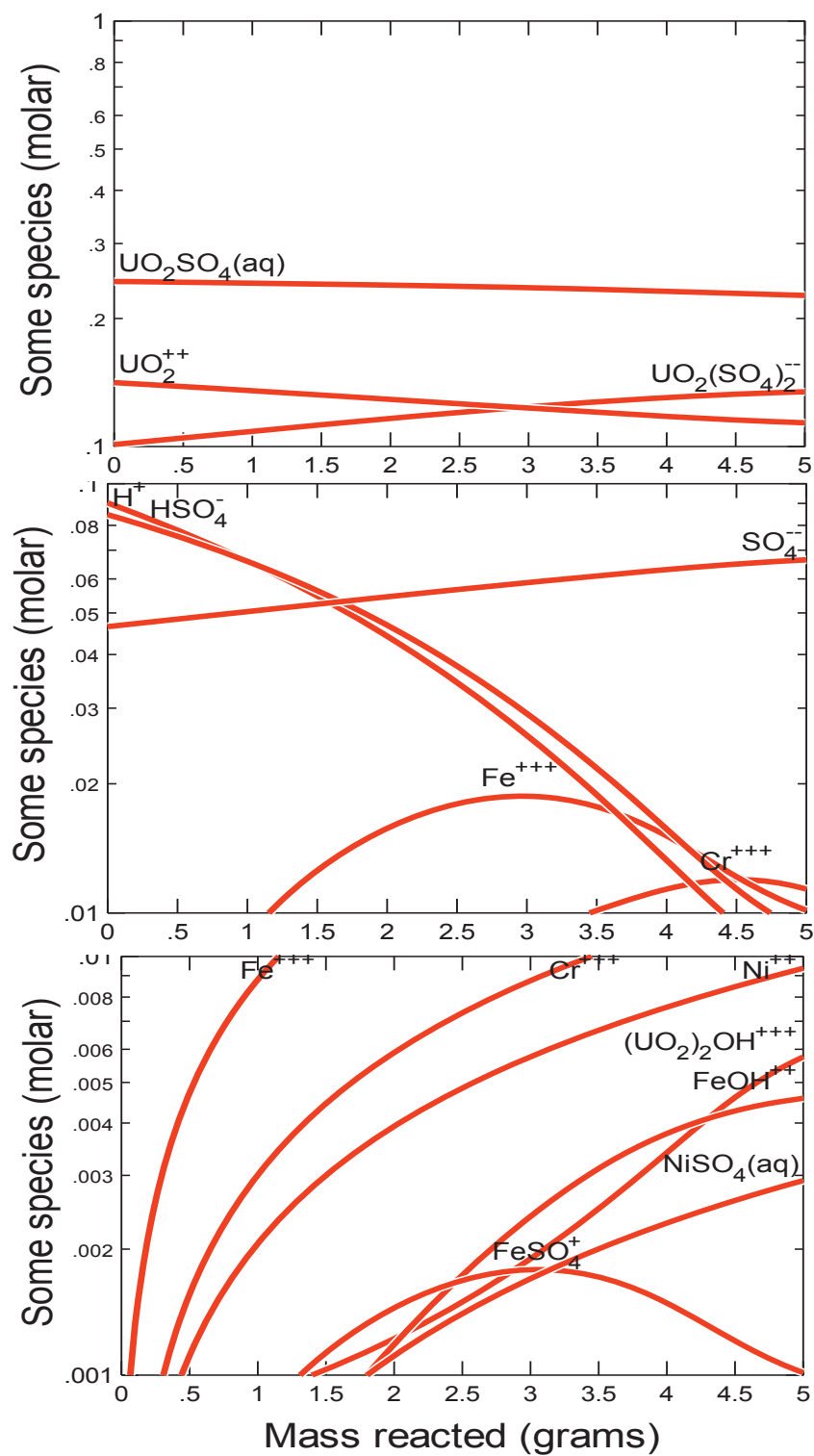


FIGURE 13 Equilibrium Model Results for the Dissolution of 316 Stainless Steel (see Table 3) in the SHINE Solution (Table 1). Plots show equilibrium species concentrations (mol/L) for the case in which mineral precipitation is suppressed. The pH for this model run is shown in the upper left plot of Figure 12.

5 CONCLUSIONS AND RECOMMENDATIONS

The results presented and discussed above are from the chemical modeling of the SHINE target solution. The saturation state of the solution was calculated, and solid phases that are thermodynamically stable (candidates for possible precipitation) under relevant conditions were identified. The aqueous speciation of the solution was also determined, as this information can be used to predict the chemical evolution of the system (pH, Eh, and saturation state) if conditions change (temperature and chemical composition). The key observations made in this study are:

- The solution is predicted to be saturated with respect to several solid phases, some of which are not expected to form due to kinetic limitations. Examples with poorly known precipitation kinetics that may need to be investigated experimentally are ZrO_2 , SnO_2 , BaSO_4 , CoWO_4 , and RuO_2 .
- Uranyl peroxide may precipitate if the steady-state concentration of radiolytically generated peroxide is maintained above a certain threshold value. Based on the limited thermodynamic data available, this threshold concentration for precipitation was found to be $3.0\text{E-}4$ mol/L.
- At temperatures above 50°C up to 100°C , the target solution is more likely to precipitate ferric iron oxides and a beryllium oxide (relative to 25°C) due to the increasing saturation indices for these minerals with increasing temperature.

It is recommended that planned experimental studies be expanded to account for key fission, activation, and corrosion products that are shown to be near or above saturation (e.g., including Zr, Sn, Ba, Co, Ru, and Fe). Experiments may be done as filtered batch type tests in which the metals are added as tracers and the equilibrated solutions passed through filters. Changes in the solution composition can be measured and any solids collected on filters can be examined by radiological scanning electron microscopy with energy dispersive X-ray spectroscopy, inductively coupled plasma-mass spectrometry (requires dissolving precipitates), and X-ray diffraction (if enough precipitate forms).

6 REFERENCES

Bethke, C. M., 2009, *The Geochemist's Workbench®*, Release 8.0 (four volumes), Hydrogeology Program, University of Illinois, Urbana, Illinois.

Bethke, C.M., 2008, *Geochemical and Biogeochemical Reaction Modeling*, Cambridge University Press, New York, 543 p.

Driscoll, J., 2014, personal communication, October 18, 2014.

Robie, R. A., Hemingway, B. S., and Fisher, J. R., 1979, "Thermodynamic properties of minerals and related substances at 298.15K and 1 bar pressure and at higher temperatures," *U.S.G.S. Bull.* 1452.

Swartout, J.A., Lane, J.A., Lind, S.C., Secoy, C.H., Bohlmann, E.G., Cullen, F.L., and Bruce, *Homogeneous Reactor Project, Quarterly Progress Report for Period Ending October 31, 1953*, Oak Ridge National Laboratory Report ORNL-1658 (1953).

Wolery, T.J., and Daveler, S.A., 1992, *EQ6, A Computer Program for Reaction Path Modeling of Aqueous Geochemical Systems: Theoretical Manual, User's Guide, and Related Documentation*, Version 7.0, Lawrence Livermore National Laboratory Report UCRL-MA-110662 PT IV.

This page intentionally left blank